An Iterative Adaptive Approach for Blood Velocity Estimation Using Ultrasound

Gudmundson, Erik; Jakobsson, Andreas; Jensen, Jørgen Arendt; Stoica, Petre

Published in:
European Signal Processing Conference

Publication date:
2010

Document Version
Early version, also known as pre-print

AN ITERATIVE ADAPTIVE APPROACH FOR BLOOD VELOCITY ESTIMATION USING ULTRASOUND

Erik Gudmundson[*], *Andreas Jakobsson*[†], *Jørgen A. Jensen*[‡], *and Petre Stoica*[*]

[*] Dept. of IT, Uppsala University, Uppsala, Sweden
[†] Center for Mathematical Sciences, Lund University, Lund, Sweden
[‡] Center for Fast Ultrasound Imaging, Technical University of Denmark, Lyngby, Denmark

ABSTRACT

This paper proposes a novel iterative data-adaptive spectral estimation technique for blood velocity estimation using medical ultrasound scanners. The technique makes no assumption on the sampling pattern of the slow-time or the fast-time samples, allowing for duplex mode transmissions where B-mode images are interleaved with the Doppler emissions. Furthermore, the technique is shown, using both simplified and more realistic Field II simulations, to outperform current state-of-the-art techniques, allowing for accurate estimation of the blood velocity spectrum using only 30% of the transmissions, thereby allowing for the examination of two separate vessel regions while retaining an adequate updating rate of the B-mode images. In addition, the proposed method also allows for more flexible transmission patterns, as well as exhibits fewer spectral artifacts as compared to earlier techniques.

1. INTRODUCTION

In medical ultrasound systems, spectral Doppler is a powerful tool for non-invasive estimation of velocities in blood vessels (see, e.g., [1] and the references therein). The data for the estimation is created by focusing the ultrasound transducer array along a single direction and sampling data at the depth of interest. The velocity of the moving blood can be estimated by illuminating the same image line repeatedly, and hereby follow the motion of the blood. Taking out a single sample from each pulse emission produces a slow-time signal sampled at the pulse repetition frequency, f_{prf}, which yields a sinusoidal signal with a frequency of

$$f_p = \frac{2v_z}{c} f_c, \tag{1}$$

where v_z is the blood velocity along the ultrasound direction, $c = 1540$ m/s is the speed of propagation, and f_c the emitted ultrasound (center) frequency (typically 3-10 MHz) [1]. A common way of estimating the blood velocity at a specific depth is to estimate the power spectral density (psd) of the sampled signal. Displaying the psd as a function of time, a so-called sono- or spectrogram, visualizes changes in the blood velocity distribution over time. Traditionally, in ultrasound imaging, the psd is estimated using the periodogram or an averaged periodogram, also known as Welch's method [2]. However, as is well-known, this approach suffers from low resolution and/or high leakage, and to achieve sufficient spectral resolution, the duration of the observation window must be long. This means that a large number of transmissions has to be used, which reduces the temporal resolution and makes it difficult to see details in the rapid acceleration phases of the cardiac cycle. Furthermore, it is generally also necessary to acquire B-mode images, allowing the operator to navigate and choose the region in which the blood velocity should be estimated. As the same system is used for both the velocity estimation and for forming B-mode images, these two transmissions are interleaved. Since it is desirable to update the B-mode images frequently to allow the operator to find and track the vessel position, it is necessary to reduce the number of Doppler transmissions.

In [3], some of the authors introduced the data-adaptive Capon- and APES-based blood velocity spectral estimation techniques, herein termed the *Blood Power spectral Capon* (BPC) and the *Blood APES* (BAPES) techniques. These techniques exploit the availability of additional fast-time measurements from neighboring depths to improve the estimators' performance, as well as make use of the recent development in high-resolution data adaptive spectral estimation techniques. A simple reformulation of BPC along the lines of [4] would also allow for an amplitude spectral Capon approach, which we here term the *Blood Capon* (B-Capon) approach. As shown in [3], these methods offer substantial improvements over the traditionally used Welch's method, allowing for an accurate estimation of the blood spectrum on drastically fewer slow-time samples as compared to the Welch's method. These results have also been confirmed in thorough *in vivo* studies [5, 6].

Recently, researchers have examined spectral estimation techniques that allow for irregular sampling schemes, so that B-mode images can be acquired in between the regular Doppler transmissions. As it is crucial to maintain the Nyquist frequency, one has to be careful when considering interleaved acquisition techniques. For example, if every second Doppler transmission is replaced by a B-mode image acquisition, the Nyquist limit is halved, reducing the velocity range by a factor of two. In [7], one of us proposed a correlation-based technique for spectral estimation, allowing for random sampling schemes; however, the method requires large sets of data and in sampling schemes with few Doppler emissions, alias occurs. Moreover, in [8], the missing samples, i.e., samples where a B-mode image was acquired instead, were reconstructed using a filter bank technique, so that a spectrogram can be estimated from a full set of data. The technique, however, reduces the velocity range in proportion to the number of missing samples.

Recently, the case of periodically gapped (PG) measurements was investigated in [9], and the B-Capon and BAPES methods were extended along the lines of [10]; these methods are here termed the BPG-Capon and the BPG-APES techniques. However, the methods in [9] are restricted to the case of periodically gapped sampling of the slow-time

 ISSN 2076-1465

data and will not work for more general irregular sampling schemes.

Typically, to allow for an adequate updating frequency of the B-mode images, about 40% of all the transmissions should be the broad-band pulses used to form the B-mode images. Furthermore, it would be beneficial if the remaining measurements could be arranged such that two different regions of interest could be examined simultaneously, for instance, allowing the medical doctor to compare the blood velocities before and after a region of stenosis in the blood vessels. These requirements, along with the desire to be able to form arbitrary sampling patterns, e.g., to allow for more or less detailed estimates in various regions, necessitate the development of improved techniques able to estimate the blood spectral density from arbitrary sampled and often sparse slow-time data.

In this paper, making use of recent work in MIMO radar systems [11–13], we propose a data-adaptive iterative blood velocity spectral estimator that allows for an arbitrary sampling of the slow-time measurement. Using both simplified and realistic Field II [14] simulation data, we show that the presented method allows for a reliable estimation of the blood velocity spectrum using only 30% of the available measurements, thus allowing for the velocity estimation at two different regions of interest, while still updating the B-mode images at an adequate pace.

Some words on notation: In the following, $(\cdot)^T$ and $(\cdot)^*$ denote the transpose and the Hermitian, or conjugate transpose, respectively. Moreover, $\mathrm{diag}(x)$ and I_N denote a diagonal matrix formed with the vector x along the diagonal and the identity matrix of size $N \times N$, respectively.

2. PRELIMINARIES

The slow-time data acquired by the spectral Doppler at depth k, corresponding to emission n, is commonly modeled as [1, 3]

$$x_k(n) = \alpha_{v_z} e^{j\phi k + j\psi_{v_z} n} + w_k(n), \tag{2}$$

where α_{v_z} is the (complex-valued) amplitude of the sinusoidal signal at frequency ψ_{v_z}, which is directly related to the blood velocity v_z as

$$\psi_{v_z} = -\frac{2\omega_c}{c f_{prf}} v_z = -\frac{2v_z}{c}\omega_c T_{prf}, \tag{3}$$

where $\omega_c = 2\pi f_c$, and T_{prf} is the time between pulse repetitions. Furthermore, ϕ is the demodulating frequency, relating the fast-time samples at each depth, defined as

$$\phi = \frac{\omega_c}{f_s}, \tag{4}$$

where f_s is the sampling frequency, and $w_k(n)$ denotes a residual term consisting of all signals at velocities different from v_z as well as additive noise. From (2) and (3), we see that the psd with respect to ψ_{v_z} is equivalent to the blood velocity distribution at the examined location, so the problem of estimating the blood velocity can be seen to be equivalent to the estimation of $\left|\alpha_{v_z}\right|^2$ for each velocity of interest. We will herein make no assumptions on the slow-time sampling pattern, nor the fast-time pattern, thus allowing for an arbitrary sampling scheme. The slow-time samples are therefore denoted $n = n_1, \ldots, n_N$, and the fast-time samples $k = k_1, \ldots, k_K$.

We will now rewrite the signal in (2), describing it as the sum of the contributions from each frequency grid point $\{\psi_{m,v_z}\}_{m=1}^M$,

$$x_k(n) = e^{j\phi k} \sum_{m=1}^{M} \alpha_{m,v_z}^{(k)} e^{j\psi_{m,v_z} n} + e_k(n), \tag{5}$$

where $n = n_1, \ldots, n_N$ and $e_k(n)$ is zero mean white complex Gaussian noise with variance η. This means that any possible noise coloring is modeled by the first term in (5), i.e., the signal part. Due to the smoothness of the blood flow profile, the blood spectral amplitude at various fast-time positions, i.e., over a range of depths, $\alpha_{m,v_z}^{(k)}$, $k = k_1, \ldots, k_K$, will be almost constant as long as the fast-time range is limited to be within the emitted pulse length. Moreover, since ϕ is known, we can proceed to demodulate $x_k(n)$ to simplify the following calculations, introducing

$$z_k(n) = e^{-j\phi k} x_k(n), \tag{6}$$

or, in a more compact form:

$$z_k = A\alpha_{v_z}^{(k)} + e_k, \tag{7}$$

where

$$\begin{aligned} z_k &= \left[z_k(n_1) \cdots z_k(n_N)\right]^T, && (8)\\ \alpha_{v_z}^{(k)} &= \left[\alpha_{1,v_z}^{(k)} \cdots \alpha_{M,v_z}^{(k)}\right]^T, && (9)\\ A &= \left[a_1 \cdots a_M\right], && (10)\\ a_m &= \left[e^{j\psi_{m,v_z} n_1} \cdots e^{j\psi_{m,v_z} n_N}\right]^T, && (11) \end{aligned}$$

and where e_k is defined similarly to z_k. From the estimate of the amplitudes at depth k, $\hat{\alpha}_{m,v_z}^{(k)}$, one may, due to the smoothness of the blood flow profile, form an estimate of the central amplitude by simply averaging the neighboring amplitude estimates:

$$\hat{\alpha}_{m,v_z} = \frac{1}{K} \sum_{k=k_1}^{k_K} \hat{\alpha}_{m,v_z}^{(k)}. \tag{12}$$

It now remains to find $\hat{\alpha}_{m,v_z}^{(k)}$, $m = 1, \ldots, M$, for which we propose the *Blood Iterative Adaptive Approach* (BIAA) algorithm.

3. THE BIAA ALGORITHM

Exploiting the similarities to the work in [11–13], we proceed to derive the BIAA algorithm. Noting that $\left|\alpha_{m,v_z}^{(k)}\right|^2$ forms a measure of the blood spectral density at velocity v_z, it is clear that the covariance matrix of the data z_k can be expressed as

$$R_{BIAA}^{(k)} = \sum_{m=1}^{M} \left|\alpha_{m,v_z}^{(k)}\right|^2 a_m a_m^* + \eta I_N = A P_{BIAA}^{(k)} A^* + \eta I_N, \tag{13}$$

where

$$\begin{aligned} P_{BIAA}^{(k)} &= \mathrm{diag}\left(\left[p_{BIAA}^{(1,k)} \cdots p_{BIAA}^{(M,k)}\right]\right), && (14)\\ p_{BIAA}^{(m,k)} &= \left|\alpha_{m,v_z}^{(k)}\right|^2. && (15) \end{aligned}$$

It should be noted that the amplitudes at neighboring depths are approximately the same, suggesting that one should form the estimate using the mean of the covariance matrices:

$$R_{BIAA} = \frac{1}{K}\sum_{k=k_1}^{k_K} R_{BIAA}^{(k)} = \frac{1}{K} A \left[\sum_{k=k_1}^{k_K} P_{BIAA}^{(k)}\right] A^* + \eta I_N. \quad (16)$$

The interference covariance matrix, i.e., the contribution from all points on the frequency grid except ψ_{m,v_z}, can now be defined as

$$Q_p = R_{BIAA} - \left|\alpha_{m,v_z}\right|^2 a_m a_m^*. \quad (17)$$

In order to find an estimate of $\alpha_{m,v_z}^{(k)}$, we consider the general linear estimator

$$\hat{\alpha}_{m,v_z}^{(k)} = h_m^* z_k. \quad (18)$$

Then, the weight vector h_m can be found by solving the following constrained minimization

$$\min_{h_m} h_m^* Q_m h_m \quad \text{s.t.} \quad h_m^* a_m = 1, \quad (19)$$

i.e., the mth weight vector is designed as a linear estimator that minimizes the output from all grid points other than ψ_{m,v_z}, while passing the component with the frequency of interest undistorted. As is readily seen, (19) is equivalent to

$$\min_{h_m} h_m^* \underbrace{\left(Q_m + \left|\alpha_{m,v_z}\right|^2 a_m a_m^*\right)}_{R_{BIAA}} h_m \quad \text{s.t.} \quad h_m^* a_m = 1, \quad (20)$$

to which the minimizer is found as (see, e.g., [2])

$$\hat{h}_m = \frac{R_{BIAA}^{-1} a_m}{a_m^* R_{BIAA}^{-1} a_m}. \quad (21)$$

An estimate of the amplitude at ψ_{m,v_z} can thus be found by inserting (21) in (18), yielding

$$\hat{\alpha}_{m,v_z}^{(k)} = \frac{a_m^* R_{BIAA}^{-1} z_k}{a_m^* R_{BIAA}^{-1} a_m}, \quad (22)$$

and an estimate over all depths can be found from (12).

It now remains to find an estimate of the noise variance η. Reminiscent of [15], we propose a method that computes the variance for each slow-time and fast-time sample, and then averages these estimates. Let $\eta_{n,k}$ denote the variance of fast-time sample k at slow-time n. The steering vector corresponding to $\eta_{n,k}^{1/2}$ is then the nth column of I_N, here denoted v_n. Consequently, an estimate of $\eta_{n,k}$ is given by [15]

$$\hat{\eta}_{n,k} = \left|\frac{v_n^* R_{BIAA}^{-1} z_k}{v_n^* R_{BIAA}^{-1} v_n}\right|^2, \quad (23)$$

and the noise variance estimate can be computed as

$$\hat{\eta}_{BIAA} = \frac{1}{NK}\sum_{n=n_1}^{n_N}\sum_{k=k_1}^{k_K} \hat{\eta}_{n,k}. \quad (24)$$

As R_{BIAA} depends on α_{m,v_z} (or, rather, $\alpha_{m,v_z}^{(k)}$), BIAA must be implemented as an iterative algorithm. Herein, we suggest to use the least squares (LS) estimate as initialization for the amplitudes:

$$\hat{\alpha}_{m,v_z}^{(k)} = a_m^* z_k / N. \quad (25)$$

The noise variance estimate can be initialized setting it to a small number, e.g., 10^{-9}. The BIAA spectral estimators are thus found by iterating the estimation of R_{BIAA} in (16), and the estimation of the amplitudes in (22), until a suitable stopping criterion is met. The amplitude estimate is then obtained through (12). See Table 1 for an outline of the BIAA algorithm.

Table 1: Outline of the BIAA algorithm

Initialize:	$z_k(n) = e^{-j\phi k} x_k(n)$, $\hat{\alpha}_{m,v_z}^{(k)} = a_m^* z_k / N$, $\hat{\eta} = 10^{-9}$,
Step 1:	$p_{BIAA}^{(m,k)} = \left\|\hat{\alpha}_{m,v_z}^{(k)}\right\|^2$,
Step 2:	$P_{BIAA}^{(k)} = \mathrm{diag}\left(\left[p_{BIAA}^{(1,k)} \cdots p_{BIAA}^{(M,k)}\right]\right)$, $P_{BIAA} = \frac{1}{K}\sum_{k=k_1}^{k_K} P_{BIAA}^{(k)}$, $R_{BIAA} = \frac{1}{K} A P_{BIAA} A^* + \hat{\eta}_{BIAA} I$,
Step 3:	$\hat{\alpha}_{m,v_z}^{(k)} = \frac{a_m^* R_{BIAA}^{-1} z_k}{a_m^* R_{BIAA}^{-1} a_m}$,
Step 4:	$\hat{\eta}_{n,k} = \left\|\frac{v_n^* R_{BIAA}^{-1} z_k}{v_n^* R_{BIAA}^{-1} v_n}\right\|^2$, $\hat{\eta}_{BIAA} = \frac{1}{NK}\sum_{n=n_1}^{n_N}\sum_{k=k_1}^{k_K} \hat{\eta}_{n,k}$.
Step 5:	Repeat Step 1–4 until practical convergence.
Finalize:	$\hat{\alpha}_{m,v_z} = \frac{1}{K}\sum_{k=k_1}^{k_K} \hat{\alpha}_{m,v_z}^{(k)}$.

Herein, we iterate until the estimates have practically converged, i.e., the difference between the amplitude estimates between two consecutive iterations is smaller than some preset threshold ε, which generally requires no more than 10-15 iterations. We note that in [15], the IAA algorithm has been shown to converge locally. All indications suggest that a similar result would hold also for BIAA.

We also note that it would be possible to form the BIAA amplitude estimate using the mean of the data over the depths, i.e., using $\bar{z} = \frac{1}{K}\sum_{k=k_1}^{k_K} z_k$, or by computing the amplitude estimates for depth k using $R_{BIAA}^{(k)}$ and not $R_{BIAA}^{(l)}$, $k \neq l$. However, the latter approach is not recommended as this would require the computation of K covariance matrices together with their inverse. Empirical studies also show that the BIAA algorithm herein proposed outperforms the version using the mean of the data.

4. NUMERICAL RESULTS

We now proceed to evaluating the performance of the proposed algorithm, first by the use of a simplified signal, where the mean squared error (MSE) of the velocity estimate from

Table 2: Parameters for transducer and femoral flow simulation

Transducer center frequency	f_c	5 MHz
Pulse cycles	M	4
Speed of sound	c	1540 m/s
Pitch of transducer element	w	0.338 mm
Height of transducer element	h_e	5 mm
Kerf	k_e	0.0308 mm
Number of active elements	N_e	128
Corresponding range gate size		123 mm
Sampling frequency	f_s	20 MHz
Pulse repetition frequency	f_{prf}	15 kHz
Radius of vessel	R	4.2 mm
Distance to vessel center	Z_{ves}	38 mm
Angle between beam and flow		60°

different estimation techniques are compared. We define the MSE of an estimate $\hat{x}$ as

$$\mathrm{MSE}(\hat{x}) = E\left\{(x-\hat{x})^2\right\}, \tag{26}$$

where $E\{\cdot\}$ is the expectation operator and x denotes the true parameter value. We will evaluate the expression in (26) empirically for different signal-to-noise ratios (SNR's), defined as $\mathrm{SNR} = \sigma_s^2/\eta$, with σ_s^2 denoting the signal energy. In the following, all data is generated using $K = 33$ regularly spaced fast-time samples, and each power spectrum consists of 500 equally spaced points in the interval $\psi_{v_z} \in [-0.5, 0.5)$. We examine the case of a sampling scheme with pattern [1 1 1 1 0 0 0 0 0 0 0 0 0], where 1 denotes an available sample and 0 that the sample is missing, due to, e.g, B-mode image acquisition or Doppler emission in another region. With this sampling pattern, it would be possible to use five of the empty sampling instances (38%) to acquire B-mode images, and the remaining four to acquire Doppler transmissions in another region. We used ten blocks of data, giving 130 sampling instances with 40 available samples. For the simplified simulations, we generated data using (5) with $P = 1$ sinusoid, having a true velocity of 0.2 m/s and amplitude $\alpha_{v_z} = 1$, and with f_c, f_s, c, and f_{prf} according to Table 2. The data was corrupted by zero mean white Gaussian circularly symmetric noise with variance η. The algorithms were then compared using the MSE of the estimated velocity. We compared the BIAA algorithm with BPG-Capon and BPG-APES from [9], having sample filter length $\tilde{N}_s = 3$ and block filter length $\tilde{N}_c = 5$. The result is displayed in Fig. 1, where we see that BIAA outperforms the other methods for lower SNR, whereas for higher SNR, all methods perform similarly.

We now proceed to a more realistic simulation, examining the same sampling pattern, but where we used the Field II program [14] to generate flow data, using the Womersley model [16] for pulsating flow from the femoral artery. The specific parameters for the flow simulation are summarized in Table 2. As customary, the stationary part of the signal was removed by subtraction of the mean of the signal. For signals taken in regions close to the vessel wall, this stationary part could be very strong, and would, if not removed, easily obstruct the blood velocity signal. Moreover, all spectrograms were produced using a dynamic range of 40 dB. The results can be seen in Fig. 2, where we also display a reference spectrogram, generated from the full data by the traditional Welch's method (see, e.g., [3, 14]), so that each vertical line is computed using 130 slow-time samples. We compared the perforamance of the BIAA algorithm with that of BPG-Capon, BPG-APES, and the autocorrelation spectrogram [7]. We see that the latter method fails, and that BPG-Capon and BPG-APES give significant artifacts in the region of high velocities. BIAA, on the other hand, shows less artifacts, still producing a clear spectrogram, closely resembling the reference spectrogram.

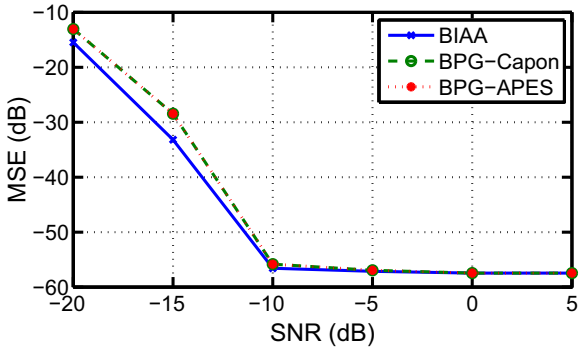

Figure 1: MSE of velocity estimate in a simplified scenario, with ten blocks of data, each with sampling pattern [1 1 1 1 0 0 0 0 0 0 0 0 0].

5. CONCLUDING DISCUSSION

In this paper, we have proposed a new algorithm for the estimation of blood velocities in medical ultrasound systems. The new algorithm can handle arbitrary sampling schemes of the data, allowing not only for duplex mode where B-mode images are interleaved with the Doppler emissions, but also for modes where two regions of the blood vessels can be interrogated simultaneously, still offering a sufficient B-mode frame rate. In such scenarios, using realistic Field II data, the proposed method was shown to provide a spectrogram containing fewer artifacts than the current state-of-the-art techniques. Simplified MSE simulations also confirmed the accuracy of the BIAA algorithm.

6. ACKNOWLEDGMENT

Some of the computations were performed using UPPMAX resources under Project p2007002. This work was supported in part by the Swedish Research Council (VR) and the European Research Council (ERC).

REFERENCES

[1] J. A. Jensen, *Estimation of Blood Velocities Using Ultrasound*. New York: Cambridge University Press, 1996.

[2] P. Stoica and R. Moses, *Spectral Analysis of Signals*. Upper Saddle River, N.J.: Prentice Hall, 2005.

[3] F. Gran, A. Jakobsson, and J. A. Jensen, "Adaptive Spectral Doppler Estimation," *IEEE Transactions on Ultrasonics, Ferroelectrics and Frequency Control*, vol. 56, no. 4, pp. 700–714, April 2009.

[4] P. Stoica, A. Jakobsson, and J. Li, "Matched-Filterbank

Interpretation of Some Spectral Estimators," *Signal Processing*, vol. 66, no. 1, pp. 45–59, April 1998.

[5] K. L. Hansen, F. Gran, M. M. Pedersen, I. K. Holfort, J. A. Jensen, and M. B. Nielsen, "In-vivo validation of fast spectral velocity estimation techniques," *Ultrasonics*, vol. 50, no. 1, pp. 52 – 59, 2010.

[6] F. Gran, A. Jakobsson, J. Udesen, and J. A. Jensen, "Fast Spectral Velocity Estimation Using Adaptive Techniques: In-Vivo Results," in *IEEE Ultrasonics Symposium, 2007*, Oct. 2007, pp. 993–996.

[7] J. A. Jensen, "Spectral velocity estimation in ultrasound using sparse data sets," *Journal of Acoustical Society of America*, vol. 120, no. 1, pp. 211–220, July 2006.

[8] S. Klingenberg Møllenbach and J. A. Jensen, "Duplex scanning using sparse data sequences," in *2008 IEEE International Ultrasonics Symposium (IUS)*, 2008, pp. 5–8.

[9] P. Liu and D. Liu, "Periodically gapped data spectral velocity estimation in medical ultrasound using spatial and temporal dimensions," in *Proceedings of the 34th IEEE International Conference on Acoustics, Speech, and Signal Processing (ICASSP)*, April 2009, pp. 437–440.

[10] E. G. Larsson and J. Li, "Spectral analysis of periodically gapped data," *IEEE Transactions on Aerospace and Electronic Systems*, vol. 39, no. 3, pp. 1089–1097, July 2003.

[11] T. Yardibi, J. Li, P. Stoica, M. Xue, and A. B. Baggeroer, "Source Localization and Sensing: A Nonparametric Iterative Approach Based on Weighted Least Squares," *to appear in IEEE Trans. on Aerospace and Electronic Systems*.

[12] P. Stoica, J. Li, and J. Ling, "Missing Data Recovery Via a Nonparametric Iterative Adaptive Approach," *IEEE Signal Processing Letters*, vol. 16, no. 4, pp. 241–244, April 2009.

[13] E. Gudmundson, P. Stoica, J. Li, A. Jakobsson, M. D. Rowe, J. A. S. Smith, and J. Ling, "Spectral Estimation of Irregularly Sampled Exponentially Decaying Signals with Applications to RF Spectroscopy," *Journal of Magnetic Resonance*, vol. 203, no. 1, pp. 167–176, March 2010.

[14] J. A. Jensen and N. B. Svendsen, "Calculation of pressure fields from arbitrarily shaped, apodized, and excited ultrasound transducers," *IEEE Trans. Ultrason., Ferroelec., Freq. Contr.*, vol. 39, pp. 262–267, 1992.

[15] W. Roberts, P. Stoica, J. Li, T. Yardibi, and F. A. Sadjadi, "Iterative Adaptive Approaches to MIMO Radar Imaging," *IEEE Journal of Selected Topics in Signal Processing*, vol. 4, no. 1, pp. 5–20, Feb 2010.

[16] J. R. Womersley, "Oscillatory motion of a viscous liquid in a thin-walled elastic tube. I: The linear approximation for long waves," *Phil. Mag.*, vol. 46, pp. 199–221, 1955.

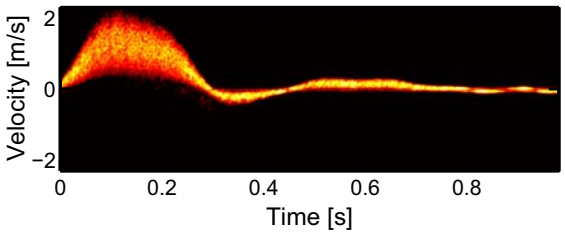

(a) Reference spectrogram

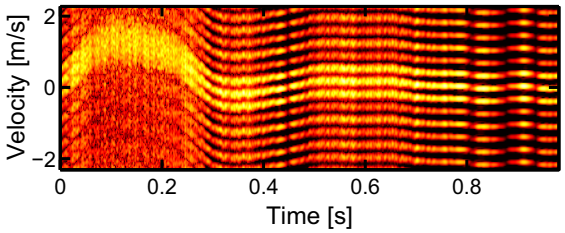

(b) Autocorrelation spectrogram

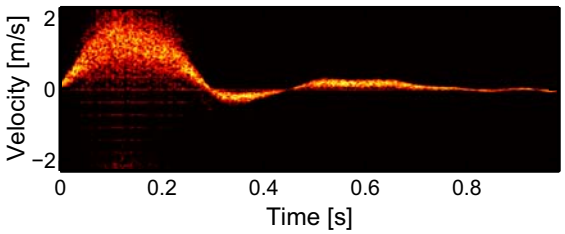

(c) BPG-Capon spectrogram

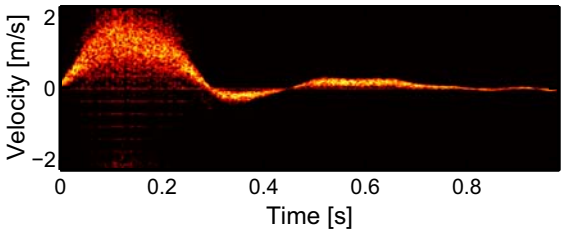

(d) BPG-APES spectrogram

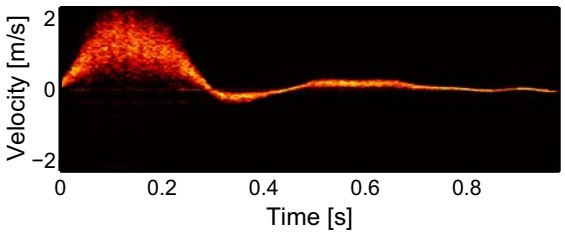

(e) BIAA spectrogram

Figure 2: (a) Traditional spectrogram (no data missing), (b) autocorrelation spectrogram, (c) BPG-Capon, (d) BPG-APES, and (e) BIAA spectrograms, for data consisting of ten blocks with pattern [1 1 1 1 0 0 0 0 0 0 0 0 0 0], with 33 fast-times samples.